

**DEVELOPMENT OF A THERMAL DESIGN MODEL FOR A
SMALL SPACECRAFT WITH AN INTEGRATED HEAT PIPE**

Madina Yensebayeva, BEng

**Submitted in fulfillment of the requirements
for the degree of Master of Science
in Mechanical & Aerospace Engineering**



**NAZARBAYEV
UNIVERSITY**

**School of Engineering and Digital Sciences
Department of Mechanical & Aerospace Engineering
Nazarbayev University**

**53 Kabanbay Batyr Avenue,
Nur-Sultan city, Kazakhstan, 010000**

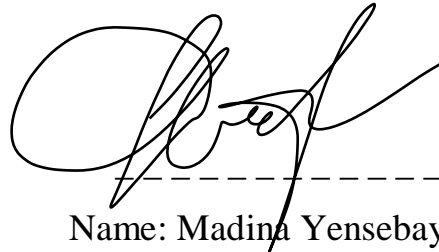
**Supervisor: Christos Spitas
Co-supervisor: Michael Yong Zhao**

April 2022

DECLARATION

I hereby, declare that this manuscript, entitled “*Development of a thermal design model for a small spacecraft with an integrated heat pipe*”, is the result of my own work except for quotations and citations, which have been duly acknowledged.

I also declare that, to the best of my knowledge and belief, it has not been previously or concurrently submitted, in whole or in part, for any other degree or diploma at Nazarbayev University or any other national or intentional institution.

A handwritten signature in black ink, appearing to read 'Madina Yensebayeva', is written over a horizontal dashed line.

Name: Madina Yensebayeva

Date: 03.04.2022

Abstract

Thermal management is essential to ensure maximum performance and mission success. The temperature conditions apply to each payload component and to the spacecraft as a whole. These specifications may include a range of operating temperatures, exceeding which may lead to deterioration or irreversible damage to a part of the satellite. Heat pipes are very useful for cooling satellites and temperature stabilization due to their lighter weight, low maintenance, and high durability. The aim of the research is to achieve a deeper comprehension of the heat pipe thermodynamic processes and design new satellite heat transfer network. For this goal, a lumped parameter model for network of heat pipes has been developed with the finite element model to conduct a combined thermal assessment and address significant technical difficulties, such as spacecraft cooling. The proposed model can be improved and used as an effective heat transfer system of the satellite in the future.

Keywords: heat pipe, lumped parameter model, heat transfer, satellite, thermal equilibrium

Acknowledgements

I express my gratitude to my thesis supervisors:

Prof. Michael Yong Zhao for all his help and valuable suggestion.

Prof. Christos Spitas for his patience, support and dedication to work, which will be a source of inspiration in my future career.

Table of Contents

Abstract	2
Acknowledgements	3
Table of Contents	4
List of Abbreviations & Symbols	6
List of Tables	7
List of Figures	8
<i>Chapter 1 – Introduction</i>	9
1.1. Background.....	9
1.2. Motivation.....	9
1.3. Research Objective.....	9
<i>Chapter 2 – Literature Review</i>	11
2.1. Overview	11
2.2. Working fluid.....	13
2.3. Transport limitations.....	15
2.4. Heat pipe advantages	17
2.5. Summary	18
<i>Chapter 3 – Methodology</i>	19
3.1. Overview.....	19
3.2. Software.....	19
3.3. Verification method.....	20
<i>Chapter 4 – Heat pipe modelling</i>	22
4.1. Geometry creation.....	22
4.2. Material properties and Mesh.....	23
4.3. Governing equation	26
4.4. Boundary condition	27
<i>Chapter 5 – Lumped parameter model</i>	29

<i>Chapter 6 – Results</i>	32
6.1.FE analysis	34
6.2.Lumped parameter model.....	38
<i>Chapter 7 – Comparison with mathematical model</i>	43
<i>Chapter 8 – Conclusion</i>	46
References	47
Appendix	51

List of Abbreviations & Symbols

CFD	Computational Fluid Dynamics
P	Static pressure
T	Temperature

List of Tables

Table 1.....	14
Table 2.....	21
Table 3.....	38
Table 4.....	41
Table 5.....	43

List of Figures

Figure 1.....	16
Figure 2.....	19
Figure 3.....	23
Figure 4.....	24
Figure 5.....	25
Figure 6.....	25
Figure 7.....	27
Figure 8.....	28
Figure 9.....	29
Figure 10.....	30
Figure 11.....	31
Figure 12.....	32
Figure 13.....	33
Figure 14.....	34
Figure 15.....	34
Figure 16.....	35
Figure 17.....	36
Figure 18.....	37
Figure 19.....	38
Figure 20.....	38
Figure 21.....	39
Figure 22.....	41
Figure 23.....	42
Figure 24.....	44

Chapter 1 – Introduction

1.1 Background

Heat pipes are passive instruments with heat transfer that employ the phase change concept of a flowing working liquid inside the heat pipe to transfer significant amounts of heat with very small changes in temperature [1]. Some of the most common varieties of heat pipes are loop, micro, pulsating and tubular heat pipes [1]. Heat pipes have a broad variety of applications, from aerospace field to thermal regulation of electronic components, due to their reliability and efficiency of a heat transfer. It is also important to mentioned that heat pipes contains closed systems that do not need any power, and their dependability originates from their adaptable, straightforward, and passive design. This, in turn, makes it a practical alternative for cooling electronics and one of the most efficient tools for maintaining temperature distribution in a satellite.

1.2. Motivation

Thermal management is essential to ensuring the mission's maximum performance and success. Temperature conditions apply to every component of the payload and spacecraft bus. These specifications might include an operation and a survival thermal gradient that, if exceeded, could result in degraded performance or irreversible damage to the part of the satellite. In case electrical equipment overheats, it will stop working correctly and may have a shorter lifespan. Battery efficiency tends to suffer if the temperature is off-nominal or a considerable temperature difference between the battery cells. Large temperature fluctuations can also cause the satellite structure to deform, potentially causing severe pointing errors. And these are just a couple of minor mission-killing issues that might arise if temperatures are not adequately controlled in the satellite.

1.3. Research Objectives

- Design a new satellite heat transfer network
- Develop a lumped parameter model for the thermal management of the satellite.

Heat pipes are very useful for cooling satellites and temperature stabilization due to their lighter weight, low maintenance, and high durability. As mentioned before, maintaining isothermal structures is critical for orbiting astronomical experiments under adverse solar heating conditions. Throughout the orbit, a spacecraft is fixed on a specific location, such as a star. As a result, one part of the spaceship is always exposed to high levels of solar radiation, while another is subjected to outer space. The idea is to design a network of heat pipes to transmit heat from the sun-heated side to the cold side of the structure, therefore balancing the temperature. This network can also be utilized in satellites to disperse heat generated by electronic parts. A numerical finite element model will be presented to perform a heat pipe thermal model simulation. Based on that a lumped parameter model will be developed further as an engineering-approach tool for the thermal management of the satellite.

The research questions are as follows:

- Is there an available heat pipe network on the concept of lumped parameter model?
- Is the lumped parameter model practical enough to manage the thermal situation inside the satellite?

Chapter 2 – Literature Review

2.1. Overview

The usage of heat pipes has grown in recent years as a result of new thermal restrictions that are making traditional cooling systems increasingly ineffective. Heat pipes, which usually operate in a phase change cycle, have a high heat transfer rate and the advantage of complete passivity. A heat pipe is made up of a sealed container, a wick structure, and an amount of liquid/vapor equilibrium working fluid. Heat is transferred externally towards the evaporation part and dissipated in the condensation area through the heat sink. The produced vapor is transported to the condenser from the evaporator due to the pressure difference between the cold and hot regions. The liquid formed as a result of condensation moves back into the evaporation region due to capillary pumping caused by the action of a wick structure.

This high effective heat transfer is produced as a result of the latent heat created and absorbed as the phase of the working fluid changes. As a result, heat pipes have to disperse heat by effectively transporting it from the evaporation to the condensation region, rather than to cool an object directly. It has gotten the most attention since it was first introduced by [2]–[6]. And practically all analytical investigations focused solely on the physics of vapor flow; due to their complexity, liquid flow part were completely neglected. [7], [8], created a dynamic heat pipe model based on energy conservation, consisting of three control volumes, one for the liquid area and the other two for the solid region, and finally computed the mathematical model for each of the three control volumes. A 1D dynamic simulation was completed and compared it to real empirical results, demonstrating that such a proposed model reduces the time needed to estimate heat pipe thermal performance. [9], investigated the thermal conductivity in the wall of the heat pipe and porous wick in the situation of a differential heat input. A 2D stationary analytical solution for a tubular heat pipe was presented by [10], [11] which included hydrodynamic

coupling among liquid and vapor . Both the empirical findings received by [12] and the numerical findings published by [13] correspond particularly well with the analytical hypothesis. Many numerical models have been developed because of the underlying difficulties in obtaining an empirically integrated solution for the complete heat pipe system. The issue of the liquid-vapor interaction was addressed by combining liquid - vapor momentum equations with the Laplace Young formula [14],[15], either by introducing a momentum jump condition [16]. [17]–[19] proved the first effort to conduct a comprehensive transient simulation of a heat pipe integrated with external steady devices. The performance of a heat pipe is modeled using a lumped parameters technique, in which the thermal conductivity in the exterior solid regions of the heat pipe in contact with the evaporation and condensation regions is estimated using an open source finite volume algorithm (OpenFOAM). To simulate the transient heat pipe behavior, [20], [21] employed a quasi-steadystate 1D a vapor flow model and study for transient 2D wall and wick heat conduction. The transient study for 2D heat wall conduction issue was efficiently addressed using a boundary element technique, and the vapor flow dynamics were determined using a numerical approach. Later on, in order to simplify heat pipe modeling, various alternative schemes were provided. Based on the analogy of an electrical network, the first transient model of a heat pipe was built by [22]. Linear ordinary differential equations of the first order have been used to describe different processes governing the behavior of a heat pipe, namely the transient thermal conductivity of the wall and stationary steam flow. When the outcomes were compared to earlier empirical observations [23], [24], they revealed only minor variations in comparison to a fully transient model. Certain essential fluid mechanics behaviors, such as the drying of the wick structure have not been well recorded, even when the fluid capacitance was relatively small in comparison to the heat capacity of the solid. To specify the actual evaporator and condenser lengths, a fluidic model of dynamic network is required to predict the gas and liquid limit levels within the heat pipe. The structural planning of heat exchangers with integrated heat pipes necessitates the estimation of such lengths. Based on the boundary condition as force balance among friction, capillary, gravity, and the effect of buoyancy on

the working fluids, a two- phase flow model is provided by [25] to analyze the nonlinear behavior of the thermodynamic response and heat flow rate. The nonlinear behavior resulting by capillary obstruction due to formation of liquid bridges is confirmed by comparison with their tests. [26] established a model for analyzing heat pipes with high temperatures in a transient two-dimensional compressible way. The wick is considered to be a uniform working fluid distribution with pure conducting medium. [27] developed a 1D computational steady-state model to examine the features of micro heat pipe as for determining the constraints of heat transmission capability with water. [28], [29] compared the heat pipe operation to a thermodynamic cycle. Since the working fluid circulates due to temperature and pressure differences, the optimal working temperature of the heat pipe might be determined by the ratio of temperature and pressure of the working fluid of the vapor phase.

2.2 Working fluid

The targeted working temperature is one of the most important factors in choosing a working fluid. Nevertheless, there are quite a lot of other aspects to examine when determining the best fluid for a certain application:

- **High latent heat** of evaporation is required to keep the pressure drop within the heat pipe as low as possible, and to transport a significant amount of thermal energy with practically no liquid consumption [30].
- **High surface tension** is required to provide a strong capillary driving force as well as to perform the heat pipe against gravitational forces.[31].
- **High thermal conductivity in wick is necessary** to decrease the radial difference in temperature as well as lower the risk of overheating within the wick or on the side walls.
- A **minimal viscosity** of liquid and vapor is required to decrease resistance to liquid flow.
- The **vapor pressure** should not be too low or high across the working temperature range to prevent excessive vapor velocities and flow disturbances.

The choice of the working fluid also relates on the numerous constraints on the heat flow happening within the heat pipe outlined in paragraph 2.3.

Furthermore, the temperature range of the working medium affects the performance limitations of the heat pipe. Table 1 lists a few different substances and their recommended operating temperatures.

Fluid	Melting point [C]	Boiling point at atmospheric pressure [C]	Operation range [C]
Methanol	-98	64	10 to 130
Toluene	-95	110	50 to 200
Ammonia	-78	-33	-60 to 100
Mercury	-95	57	0 to 120
Ethanol	-112	78	0 to 130
Acetone	-95	57	0 to 120
Helium	-271	-261	-271 to -269
Nitrogen	-210	-196	-203 to -160
Water	0	100	30 to 200

Table 1. Working fluids operational range

The working fluid in the most of heat pipes for satellite systems and electronics cooling is Ammonia, Methanol, or Water. [32]–[34]. Ammonia has the optimum thermodynamic properties, making it an effective heat pipe working fluid, therefore it was taken as a working fluid for simulation.

2.3. Transport limitations

The temperature of the heat pipe must be regulated based on the cooling circumstances. If the working fluid is heated above a certain temperature, it completely evaporates while preventing the condensation process. [35]. Furthermore, the working fluid can not phase change below a specific temperature, and the thermal conductivity will indeed be minimized. The lower temperature range is usually the few degrees above the operating fluid's freezing point. The constraints that cause the heat pipe to fail are defined by insufficient fluid flow into the evaporator at a specified heat release, which leads to drying of the wick structure of the evaporator.

Capillary, entrainment and boiling constraints are the most essential restrictions in terms of maximum heat input.

- When the generating capillary pressure is not enough to enable sufficient flow of fluid from the condensation to the evaporation, the capillary limit happens, leading the evaporator wick to dry out. [20][4]. In most cases, the capillary limit is a heat pipe's main heat transmission constraint.
- The boiling constraint happens while the temperature reduction over the whole structure of the wick in the evaporation area changes with the heat flow of the evaporator. The breakpoint is achieved once the difference in temperature surpasses the degree of superheat that can be sustained under nucleate boiling circumstances. This causes vapor bubbles that partly obstruct the return of the fluid and may lead to drying of the evaporator wick.
- The term "entrainment limit" describes a situation where the vapor generates large shear forces when moving in the opposite direction along a wick saturated with liquid, respectively the fluid is entrained by vapor and redirected to the condenser [36]. This prevents fluid from flowing into the wick structure.

Various factors (such as viscous, sonic, and condenser constraints) result in ineffective loss in performance, raising the heat pipe's working temperature.[37].

- The sonic constraint occurs at a lower thermal densities, and the related flow rate in the pipe might lead to extremely high vapor flow velocity, potentially blocking up the steam pipe.[38].
- Radiation or natural convection in a condensation region is one of the fundamental limits of a condenser. If we consider radiation cooling, then factors such as operating temperature, the surface area of the condenser and the radiation coefficient can regulate transportation through the heat pipe. [39].

By combining individual limits, it is possible to determine the temperature range at which the heat pipe will function effectively. Based on these results, the design can be significantly improved and the maximum output of the heat pipe can be known in advance.

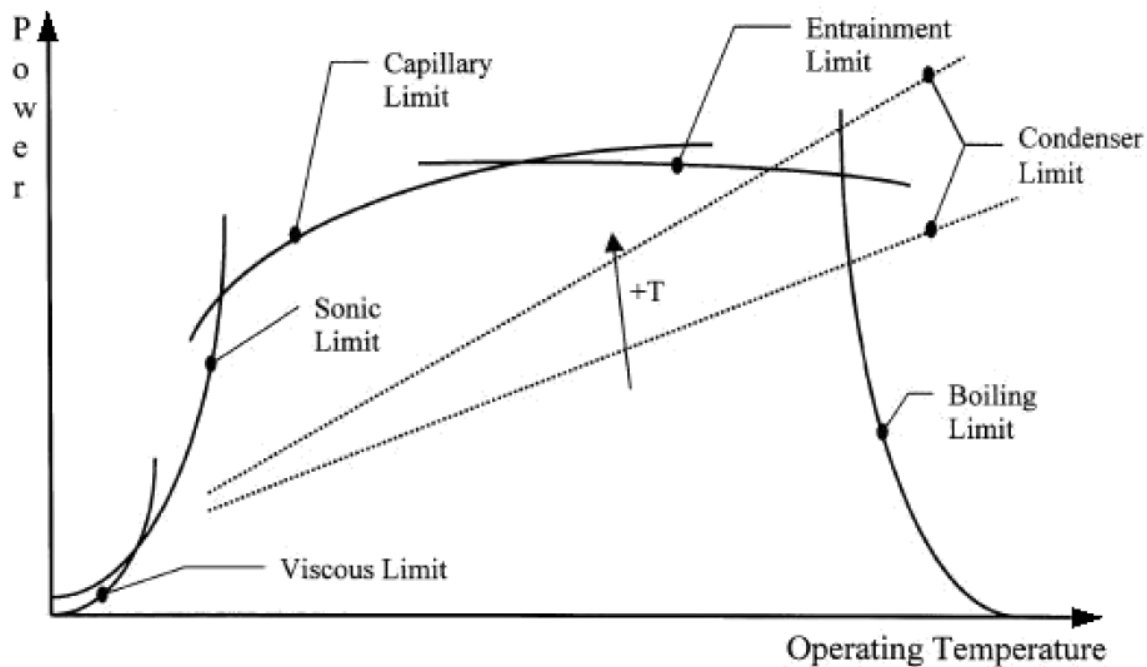


Figure 1. Transport limitations . Adapted from [40]

2.4. Advantages

Heat pipes provide a number of benefits over standard single-phase systems, making them appealing in a variety of heat transfer applications. The following are the primary characteristics:

- **High heat capacity** related to the phase shift of the operating fluid. As compared to single phase systems, the heat generated that may be transferred is frequently numerous orders of magnitude more.
- **Passive device.** Beside the heat that has been transported, they do not need any external power. Heat pipes do not contain moving components, as for example, fans, which are used for moving the working fluid in conventional models. Respectively this makes them more efficient, entirely silent and non-vibrating.
- **Coefficient of heat transmission is high.** Subsequently, heat pipes can practically isothermally function independently of fluctuations in the thermal load.
- **Variable thermal conductivity.** The efficient heat conductivity tends to increase with length and varies depending on the transmitted power and the size of the evaporator and condenser.
- Working fluids may operate at a broad range of temperatures.
- In comparison with single-phase liquid or gas processes, lower mass flow rates are needed for a particular range of temperature to transmit similar quantity of heat. A single-phase system's thermal power is defined by variations in the temperature of the operating fluid; consequently, to transmit a significant quantity of heat, a wide temperature difference or high mass flow is necessary [41].
- **Compact design size and small weight.** Since the operating fluid is thermodynamically saturated, the heat pipe functions in an almost isothermal state, which has the benefits of effectively carrying high quantities of heat, minimizing the total heat transfer region and compliance with the weight of the system.
- **Shape versatility.** The tendency to flexibility and accessibility in various sizes and shapes is one of the essential advantages of heat pipes. (see Figure 2.6). Pipes may be

made even more versatile through integrating an elastic bellows part, if any range of motion is needed.

- **Work reversibility.** The heat pipe's symmetrical construction allows it to move heat indistinctly between one side to the other based simply on the location of the heat source

2.5. Summary

The following key observation is noted after literature review:

- The temperature of the heat pipe must be regulated based on the cooling circumstances in order to avoid the complete condensation or liquidation of the heat pipe itself.
- The working fluid in the most of heat pipes for satellite systems and electronics cooling is Ammonia or Methanol.
- Heat pipes provide a number of benefits over standard single-phase systems, making them appealing in a variety of heat transfer applications.
- Lumped parameter model haven't been done in case of thermal regulation of the satellite.

Chapter 3 – Methodology

3.1. Overview



Figure 2 . Overall process

- A literature review needs to be carried out in order to answer the first RQ
- Making a workable model in Simulink for a heat pipe and verify the thermal performance using Taguchi Orthogonal method.

Since the structure will consist not just of one heat pipe, there will be a network of heat pipes. It is not practical to make a complete Finite Element Analysis of the complex flow inside the heat pipes, heat and mass transfer; that is why there will be a need to go to a simplified methodology like using a lump parameter model. It is potentially interesting regarding the model itself since it is not being done on a heat pipe network, at least not in the satellite case. Secondly, it is efficient when there is a complex network or topology because it keeps the whole system computationally manageable.

3.2. Software

Computational analysis of a heat pipe can be quite difficult, since the physical processes of a heat pipe need a highly non - linear system of partial differential equations in time, temperature ,pressure, velocity and spatial variables. COMSOL Multiphysics is a software package for modeling physical phenomena that includes several built-in equations, allowing us to focus on the physical processes rather than programming difficulties. Therefore it was used to find a finite element approximation to the system's solution and to run numerical tests on the model. Computer

simulation of this simplified steady state model aims to provide a platform for future work that will involve more complex and accurate time dependent computations.

The lumped parameter model is implemented in the MATLAB/Simulink. Simulink is a MATLAB tool that allows to quickly model complex systems and, in general, one of the effective tools for solving electric circuit problems. One of the advantages of MATLAB/Simulink is a wide range of "toolboxes" or simulation models that can be used so that each block does not require coding.

3.3. Verification method

3.3.1. Taguchi method

The construction of an Taguchi orthogonal array is a sort of standardized factorial design. The method is regulated to guarantee that all levels of all components are recognized equally. [42]. As a result, regardless of the fractionality of the design, the elements can be investigated independently of each other. The Taguchi technique has the advantage of emphasizing the average value of the specific parameter close to the desired number rather than the value between specific defined parameters, hence enhancing quality of the product. Moreover, Taguchi's experimental design method has simple structure and easy to adapt to a variety of engineering challenges, making it an effective but basic tool to use. The common L8 orthogonal array defined by Taguchi is shown in Table 2. Only these formulations are used to correctly identify the parameters.

No.	Factors						
	A	B	AB	C	D	BC	E
1	1	1	1	1	1	1	1
2	1	1	1	2	2	2	2
3	1	2	2	1	1	2	2
4	1	2	2	2	2	1	1
5	2	1	2	1	2	1	2
6	2	1	2	2	1	2	1
7	2	2	1	1	2	2	1
8	2	2	1	2	1	1	2

Table 2. Orthogonal array example

3.3.2. Response surface method

The response surface method (RSM) is a statistical methodology that consists of three stages. [43]. The first stage involves scanning investigations and setting the boundaries of the empirical domain to identify independent variables that have a substantial impact on the process. The second stage involves the use of mathematics and statistics for empirical data gained by fitting the polynomial function and assessing the system's suitability. The final step includes determining the requirements and the possibility of changing the direction to the optimal zone, as well as choosing the best parameter values. Equation 1 is represented as follows:

$$Y = \beta_0 + \sum_{i=1}^k \beta_i X_i + \sum_{i=1}^k \beta_{ii} X_i^2 + \sum_i \sum_j^k \beta_{ij} X_i X_j + \varepsilon$$

Using Equation 1 as a guide ,Y denotes the expected reaction (R_a and R_z), X_i and X_j indicate variables, β_0 indicates constant, β_i , β_{ii} and β_{ij} represents linear, quadratic and the second-order terms, correspondingly and k denotes the number of independent factors and ε is the error term.

Chapter 4 –Heat Pipe Modelling

As it was mentioned before, since there is a need to calibrate lumped parameter model, the FEA analysis of a heat pipe in COMSOL Multiphysics needs to be carried out first. Computational analysis of a heat pipe is a difficult process since its functionality is associated with complex physics. Following are the main three regions along the heat pipe: an evaporation area caused by the source of heat coming into touch with the heat pipe, the adiabatic region is located between the evaporation r and the condensation region, but is not directly connected to either the heat source or the heat sink, and the condensation region is formed by an external heat sink. The following is a specification of how an HP operates on a regular basis:

1. The higher temperatures generated in the evaporation zone caused by the source of heat cause the working liquid in a pipe to evaporate.
2. ΔP_v created by emerging vapor drives the vapor towards the condensation zone.
3. Because of the lower temperatures sustained by the heat sink, vapor condenses in the condensation region and flows down into the wick.
4. The phase is completed when the condensed working fluid in the wick reaches the evaporation area by a capillary effect ΔP_c .

4.1. Geometry creation.

Heat pipes come in a range of shapes and sizes. Tubular ones, on the other hand, are certainly the most widespread. An axisymmetric design of a copper pipe with a porous wick and a vapor chamber will be examined here. The bottom of the heat pipe contains a contact area that must be linked to the heat source to be removed. A identical contact surface for a heat sink is being used in the pipe's top. The latter is frequently associated with a finned metal.

The following simplifying assumptions was made for our numerical simulations:

- Stationary analysis was performed where the temperature and the flows are in equilibrium.

- The pipe is assumed to be horizontal, thus ignoring the effect of gravity.
- Radiation is ignored due to the low temperature difference in the heat pipe.

Parameters			
Name	Expression	Value	Description
r_outer	10[mm]	0.01 m	Outer diameter of pipe
w_casing	1[mm]	0.001 m	Casing thickness
w_wick	2[mm]	0.002 m	Wick thickness
length	150[mm]	0.15 m	Pipe length
r_inner_ca...	r_outer-w_casing	0.009 m	Inner radius of wall
r_wick	r_inner_casing-w_wick	0.007 m	Inner radius of wick
wick_poro...	0.5	0.5	Volumetric void fraction i...
wick_per...	1e-9[m^2]	1E-9 m ²	Permeability of wick
Q_in	30[W]	30 W	Heat source load
h_conv	1200[W/(m^2*K)]	1200 W/(m ² ·K)	Convection coefficient he...
l_heatsink	1[cm]	0.01 m	length of heat sink after r...
l_heatsour...	1[cm]	0.01 m	length of heat source aft...
w_contact	1.5[mm]	0.0015 m	Contact Surface Thickness
phi_in	Q_in/2/pi/(r_outer+w_contact)/l_heatsource	41519 W/m ²	Heat flux in
p_ref	1[bar]	1E5 Pa	Reference Pressure
mesh_fact...	1.0	1	Decrease to obtain a fine...
Temp_src	343.15[K]	343.15 K	Source Temperature
Temp_snk	210.15[K]	210.15 K	Sink Temperature
area	(2*pi*(r_outer+w_contact)*l_heatsource)	7.2257E-4 m ²	

Figure 3. Parameters of a heat pipe

Based on parameters, a 2D axisymmetric design of a cylindrical heat pipe was created. The dimensions of the heat pipe were as per the actual as shown in Figure 3. Copper is the containing material, and ammonia is the working fluid. Simulations was performed on a cylindrical heat pipe which was 150 mm in length.

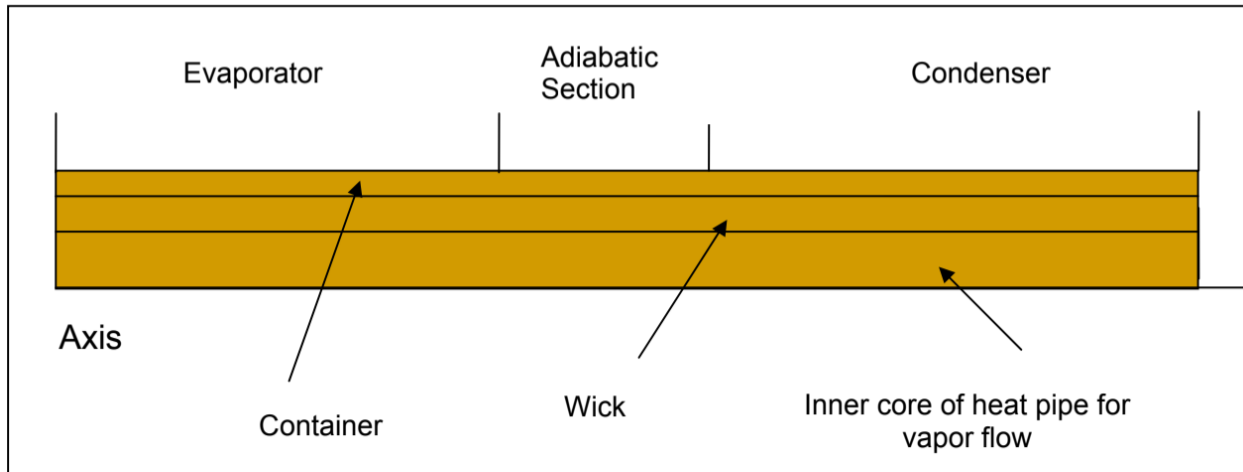


Figure 4. Heat pipe configuration

A cylindrical heat pipe is formed by revolving the rectangle below about its axis. The exterior boundaries are located at the pipe's ends as well as on the container.

4.2. Material Properties and Mesh

The **Thermodynamics** node is used to create material properties. In the wick, a vapor system based on the ideal gas law is established, whereas a liquid system based on IAPWS models is developed for the fluid phase. For the liquid system, a vapor pressure function is designed to characterize the saturation pressure. Two materials are constructed using the Generate Material option in the thermodynamic system to simply apply the properties to the model. For the pipe wall characteristics, copper from the material library is utilized.

Quadrilateral mesh for the centre part of the heat pipe and triangular meshes for the ends was used. Mesh control edges were developed to facilitate this mesh transition. The convenience of this feature is that these can be referenced during meshing, while not contributing to splitting of domains in other contexts(see Figure 5).

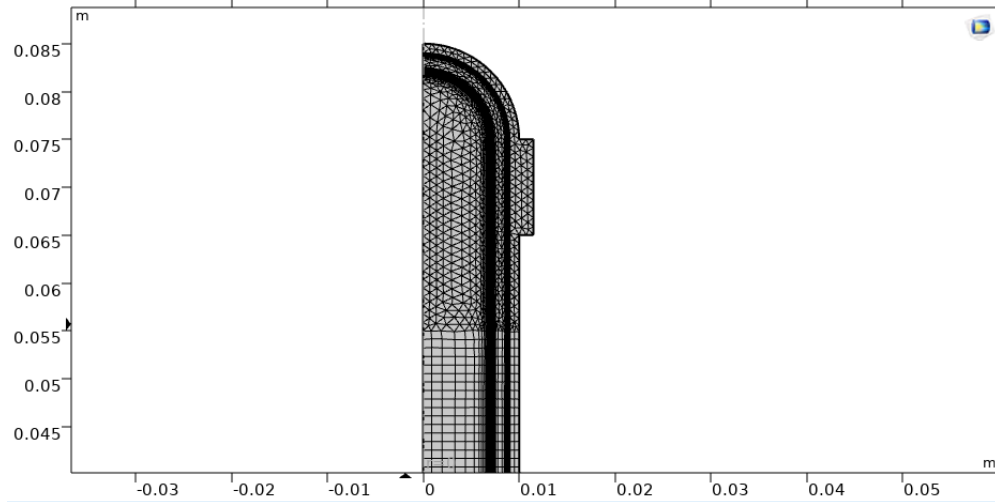


Figure 5. Mesh visualization

Mesh convergence was done by increasing the number of elements while keeping the mesh configuration same throughout the study. While increasing the number of elements, the solution outputs are converged to a specific value (see Figure 6).

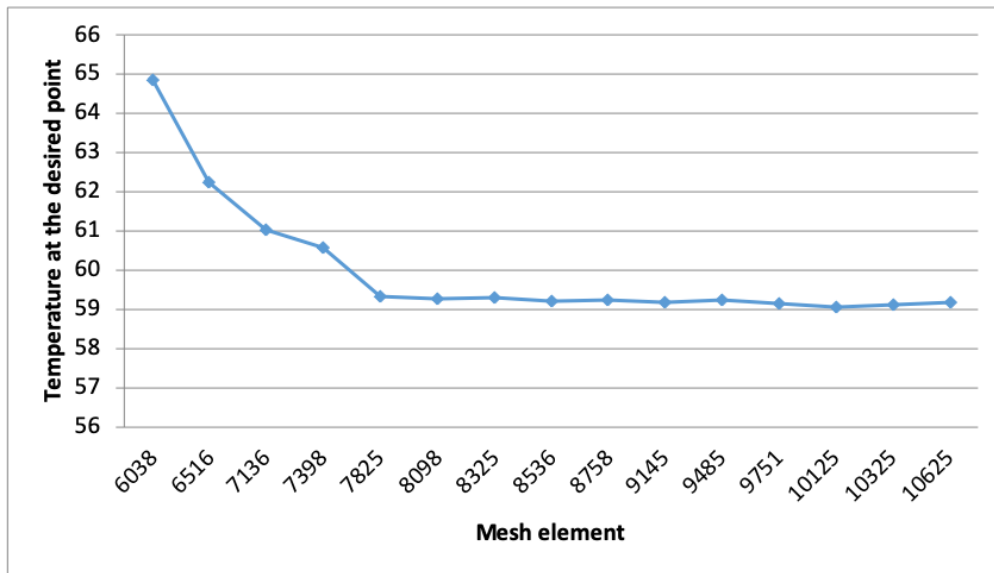


Figure 6. Mesh convergence

Next, **Materials** for the metal casing and the wick, as well as for the working fluid

(both ingaseous and liquid form) is added. Copper will be added from the built-in materials. Two thermodynamic systems are built for water vapor and liquid ammonia, which are then used to generate materials. It should be noted that there is a need to add copper to global materials for it to be accessible in the porous material node, which will be added to Component 1. A material link will be added to Component 1 to use this global Copper material for the Solid Copper Tube Casing domain selection.

4.3. Governing equation

The Navier-Stokes equations, the energy equation and the continuity equation was used for this case.

$$\rho_l \left(U_r \frac{\partial U_r}{\partial r} - \frac{U_\phi^2}{r} + U_z \frac{\partial U_r}{\partial z} \right) = -\epsilon \frac{\partial P}{\partial r}$$

$$+ \mu \left(\frac{\partial^2 U_r}{\partial r^2} + \frac{1}{r} \frac{\partial U_r}{\partial r} - \frac{U_r}{r^2} + \frac{\partial^2 U_r}{\partial z^2} \right) - \frac{\mu \epsilon}{K} U_r - \frac{C_F}{\sqrt{K}} |V| U_r$$

$$\rho_l \left(U_r \frac{\partial U_\phi}{\partial r} + \frac{U_r U_\phi^2}{r} + U_z \frac{\partial U_\phi}{\partial z} \right) = \mu \left(\frac{\partial^2 U_\phi}{\partial r^2} + \frac{1}{r} \frac{\partial U_\phi}{\partial r} - \frac{U_\phi}{r^2} + \frac{\partial^2 U_\phi}{\partial z^2} \right)$$

$$- \frac{\mu \epsilon}{K} U_\phi - \frac{C_F}{\sqrt{K}} |V| U_\phi$$

- *Energy equation:*

$$U_r \frac{\partial T}{\partial r} + U_z \frac{\partial T}{\partial z} = \alpha_{\text{eff}} \left(\frac{\partial^2 T}{\partial r^2} + \frac{1}{r} \frac{\partial T}{\partial r} + \frac{\partial^2 T}{\partial z^2} \right)$$

- *Continuity equation:*

$$\frac{\partial U_r}{\partial r} + \frac{U_r}{r} + \frac{\partial U_z}{\partial z} = 0$$

- *Navier-Stokes equations:*

$$\rho_l \left(U_r \frac{\partial U_z}{\partial r} + U_z \frac{\partial U_z}{\partial z} \right) = -\varepsilon \frac{\partial P}{\partial z} + \mu \left(\frac{\partial^2 U_z}{\partial r^2} + \frac{1}{r} \frac{\partial U_z}{\partial r} + \frac{\partial^2 U_z}{\partial z^2} \right) - \frac{\mu \varepsilon}{K} U_z - \frac{C_F}{\sqrt{K}} |V| U_z$$

4.4. Boundary Condition.

For both end the velocity will be zero. In the centerline we don't have any vertical velocity. For the liquid-vapor interface the continuity equation denotes as all the amount of liquid transferred to vapor. The mass flow rate of liquid is equal to the mass flow rate of vapor. Wick wall interface is conduction heat transfer, velocity is set to be zero because of the no slip condition. And no any fluid is transferred this line, because the other side is solid, so the continuity equation is zero. Outer pipe wall, In the adiabatic section we have no temperature difference (see Figure 7).

N°	Locations	Evaporator	Adiabatic	Condenser
1	Both ends of HP	$u = v = 0$		$u = v = 0$
2	Centreline of HP	$v_v = 0, \frac{\partial v_v}{\partial y} = 0, \frac{\partial T_v}{\partial y} = 0$		
3	Liquid-vapour interface	$\rho_v v_v = \rho_l v_l$		
4	Wick-wall interface	$u_l = v_l = 0, \rho_v v_v = \rho_l v_l = 0$		

Figure 7. Boundary condition of the heat pipe

A **Laminar Flow** interface is used to solve for the laminar flow in the vapor cavity. It is subjected to single boundary condition, apart from the axial symmetry line. At the cavity–wick contact, the pressure is designed to be the same as the saturated vapor pressure.

$$p = p_{NH_3,sat}(T)$$

It denotes that the liquid and vapor phases are claimed to be in balance in this condition. The rise in vapor pressure with temperature is what causes the vapor to move from a higher to lower temperature zone. A **Brinkman Equations** interface is utilized to simulate the circulation of liquid in a porous wick.

The pressure level is fixed using a pressure point constraint on the solid wall in the middle of the geometry. It was used to resolve the pressure field within the domain. A coupled solver was used, therefore boundary condition can be considered as suitable.

A **Heat Transfer in Porous Media interface** is utilized for transmission of a heat throughout the structure, including a vapor cavity, wick, and tube wall. It has property characteristics for every type of domain. The two Temperatures (at the heat source and heat sink) was taken as an independent variable and used in the parametric study. Parametric sweep is applied to scan a 3 parameters (T_{sink} and T_{source} length of the heat pipe) over a range of values (see Figure 8).

Parameter name	Parameter value list	Parameter unit
Temp_src (So)	range(320.15,20,400.15)	K
Temp_snk (Sir)	range(130.15,20,230.15)	K
length (Pipe l)	150,500,1000,1500	mm

Figure 8. Parametric study values

Chapter 5 – Lumped parameter model

Before building the lumped parameter model, it is important to propose the schematic of the heat transfer through the satellite. [44] was taken as a benchmark for future work. The satellite scheme in [44] constructed in such a way that the electronics subsystem is not attached to the heat source and it is considered that heat is released from these components. The heat pipe network scheme for the satellite in this study was constructed as follows(see Figure 9). Firstly, the heat is radiated to the heat storage which starts storing heat energy inside till reaching the steady state, at this point, the temperature of this subsystem is fixed at 80°C (assumed temperature) and all the heat, radiated to it, is translated to the battery through heat pipe. After that, part of this heat is translated to the camera and the rest is drained to the cold plate, the translated heat to the camera is also diverted to the cold plate through heat pipe. The other subsystems (ADCS, OBC and EPS) use the generated heat due to their operation to keep their temperature at a specific point, then, at the equilibrium, this heat is translated to the cold plate. The cold plate temperature is kept at 0°C , and all the heat flow rate translated to it is reradiated to the outer-space due to the equilibrium.

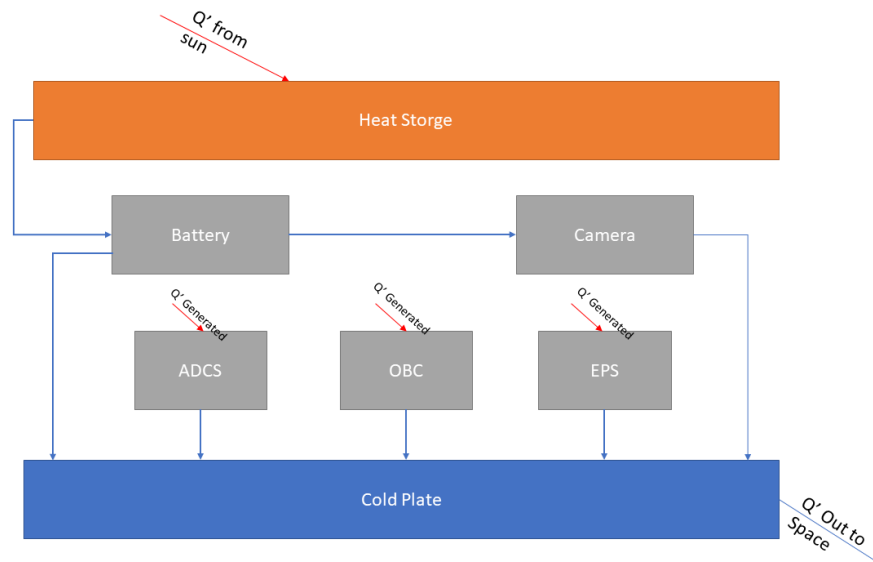


Figure 9. Satellite Heat Pipe Network Schematic

A lumped parameter model simplifies the execution of distributed physical processes, such as electrical circuits, by converting them into a topology of discrete objects that resemble the reaction of a distributed system under certain assumptions. For this network of heat pipe ,the model is made at steady state using MATLAB SIMULINK. The key point for this analysis is that each subsystem in the model is at thermal equilibrium so the heat flow rate and temperature of them can be calculated based on that.

The following table shows the operational range of each subsystem (Table 4) [46]. The lumped parameter model will be modeled in a way to satisfy this range.

Subsystem	Min. Operating temp. (°C)	Max. Operating temp. (°C)
Battery	0	45
Camera	0	45
ADCS	-50	60
OBC	-40	85
EPS	-40	105

Table 4 . Operation Temperatures for subsystems.

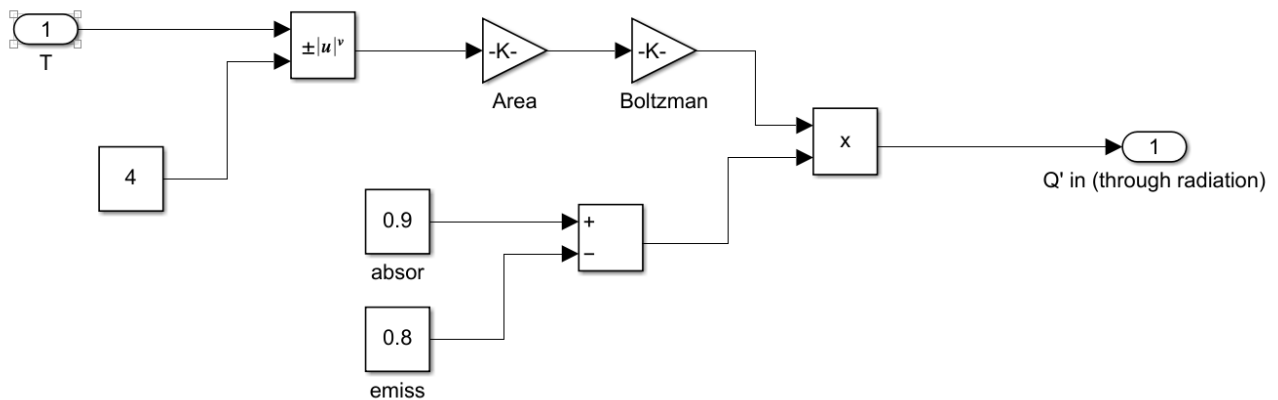


Figure 10. Heat storage subsystem

Figure 10 shows the schematic for the process of the heat radiation from the sun to the heat storage, it representing the following governing equation:

$$Q' = (\alpha - \epsilon)\sigma AT_h^4$$

Where,

$\alpha = 0.9$ (the heat storage absorptivity)

$\epsilon = 0.8$ (the heat storage emissivity)

$\sigma = 1.38064852 \times 10^{-23} \text{ m}^2 \text{ kg s}^{-2} \text{ K}^{-1}$ (Boltzman Constant)

$A = 0.202 * 0.3 \text{ m}^2$ (the surface area of heat storage)

$T_h = 80^\circ \text{C}$ (the temperature of the heat storage)

$Q' = 24 \text{W}$ (heat radiated to the heat storage)

First of all, the heat is radiated to the heat storage from the sun, further, this subsystem starts storing heat energy and its temperature starts increasing till reaching the steady state at 80°C . After that, the coming heat flow rate will equal the exiting flow rate to satisfy the equilibrium at steady state. This heat is translated to the battery through heat pipe of 150 mm.

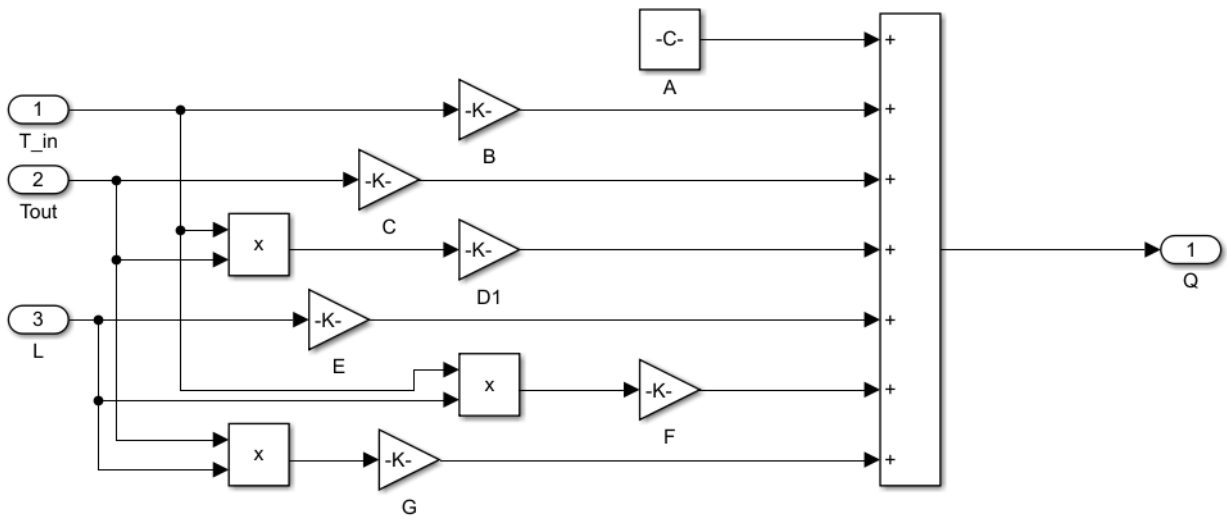


Figure 11. Heat pipe subsystem

The heat pipe is modeled in the Simulink model using estimated algebraic equation (mathematical model section), and it has 3 representations. The first, T_{in} , T_{out} and L are

inputs for the model and Q' is the output (Figure 11). The second representation, Q' , T_{in} and L are inputs and T_{out} is the output (Figure 12). The final representation, T_{out} , Q' and L are inputs and T_{in} is the output (Figure 13).

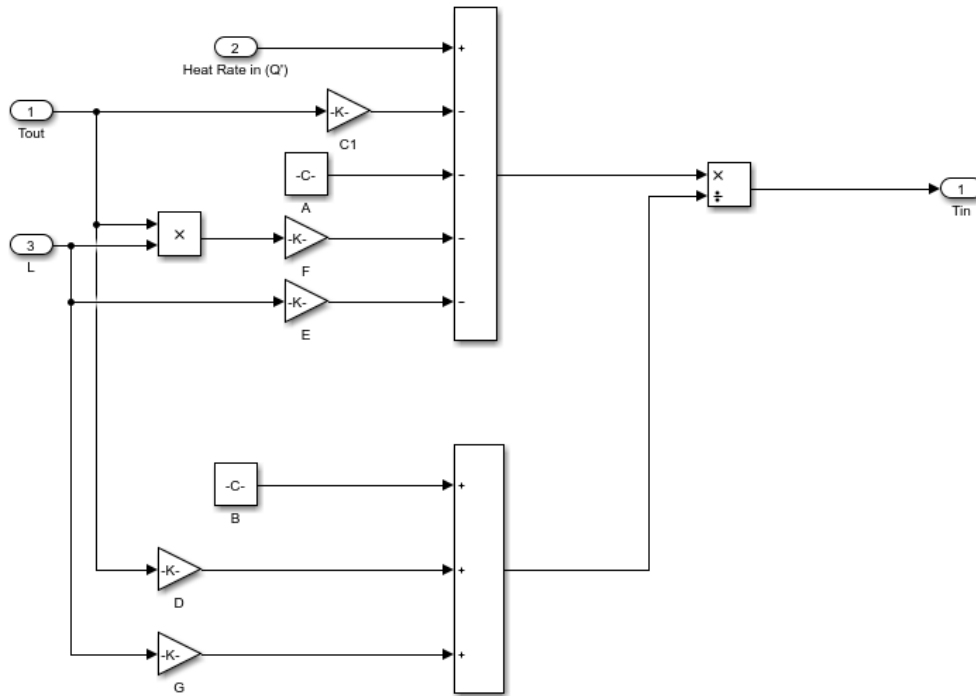


Figure 12. Heat pipe subsystem

Figure 12 shows the last representation for the heat pipe. In this representation, the input is T_{out} , L & Q' which result an output parameter of T_{in}

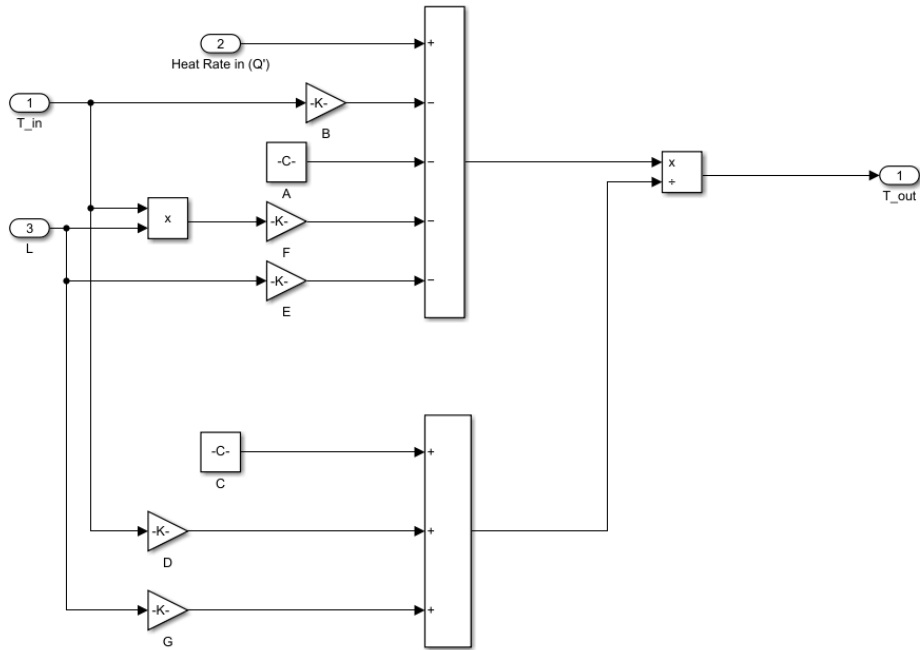


Figure 13. Heat pipe subsystem

The second representation for the Heat pipe is shown in Figure 13. The inputs here are T_{in} , L and Q' . similar to the first one, The mathematical operations are done on the input parameters to find the output (T_{out}).

Chapter 6 – Result

6.1. FE analysis

In general, as it was noted in paragraph 4.2., in the simulation the heat transfer node (for both solid and fluid) was coupled with laminar flow and flow within the wick was defined by Brickman's Equation, which was also coupled with heat transfer node. The laminar node was coupled with heat transfer node where the flow is driven by buoyant effects and pressure boundary condition. For flow Brickman node is coupled with heat transfer and for flow inside porous media also influenced by Energy. The source term was defined in the heat transfer node which accounts for phase change.

The temperature of heat pipe with dry wick as a result is shown in Figure 14 below. The heat source has a much greater temperature than the heat sink. Such a maximum temperature would be problematic in an application with temperature sensitive parts.

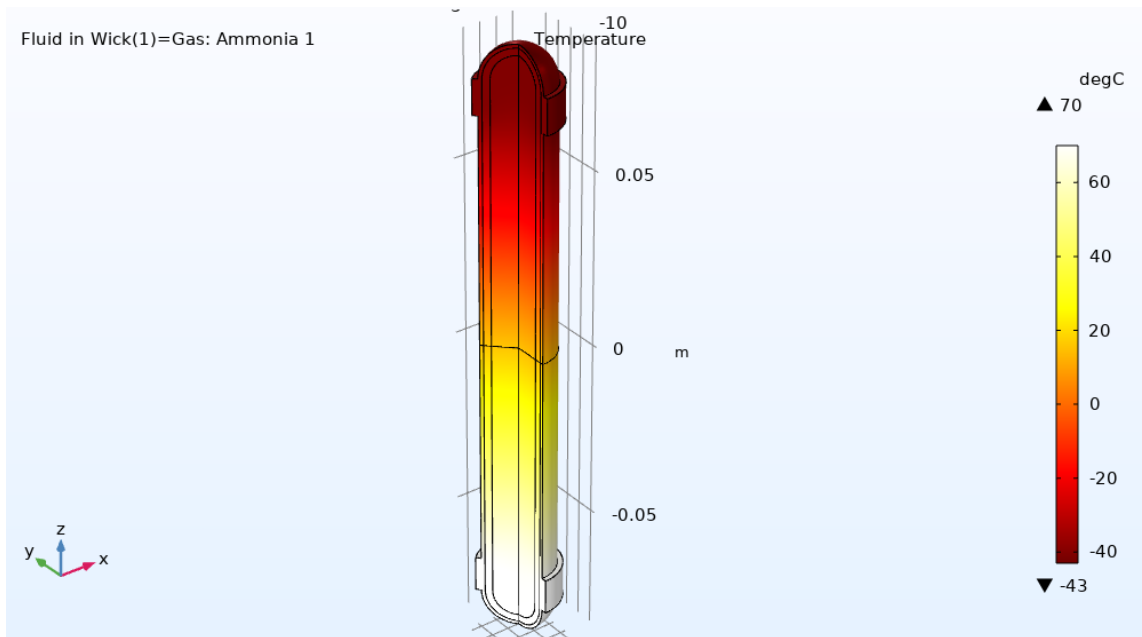


Figure 14. Temperature of heat pipe with dry wick.

The wick is considered to be saturated with ammonia in the second phase of the study, which corresponds to a heat pipe flowing at its design position. Figure 15 shows the output temperature profile, which is drastically different. Ammonia is usually in gaseous state, but at temperature below -33°C it turns liquid. The lowest temperature in the heat sink is set by -43°C, which is above the boiling point.

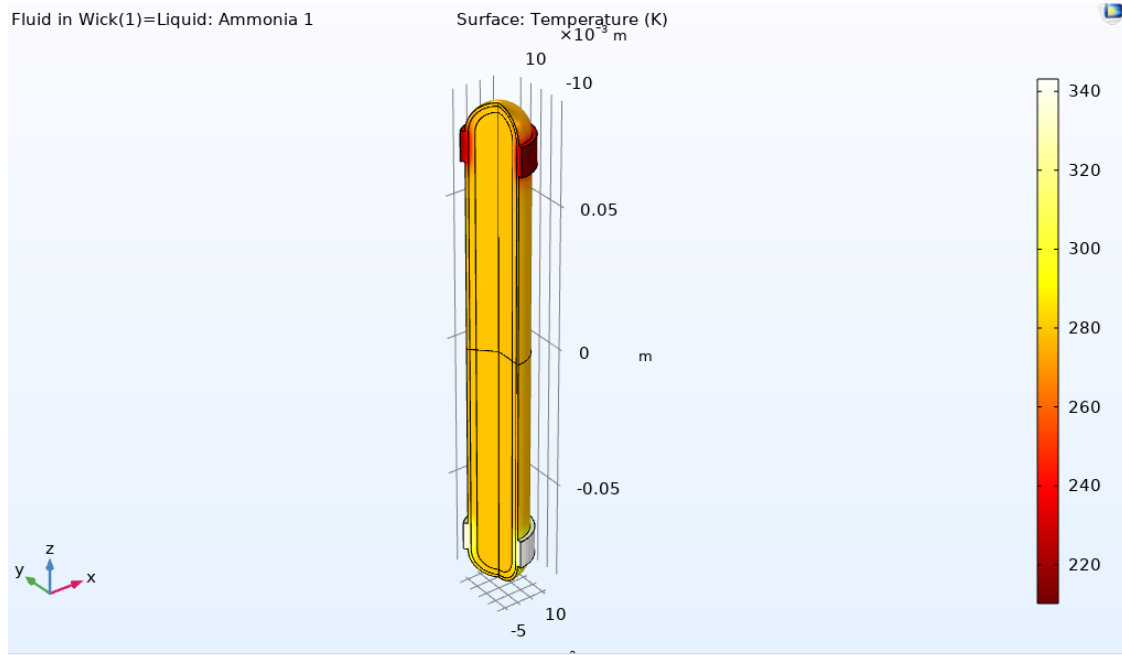


Figure 15. Temperature of heat pipe with saturated wick.

The velocity magnitude contour computed for the vapor zone and displayed in Figure 16. Since the pressure difference between the condenser and evaporator parts drives the flow through the adiabatic section, the maximum velocity magnitude occurs there. The velocity of the working fluid reduces nearly to zero in both the evaporation and the condensation parts since fluid gets stopped, heated, and cooled in the corresponding section to force it to change its phase.

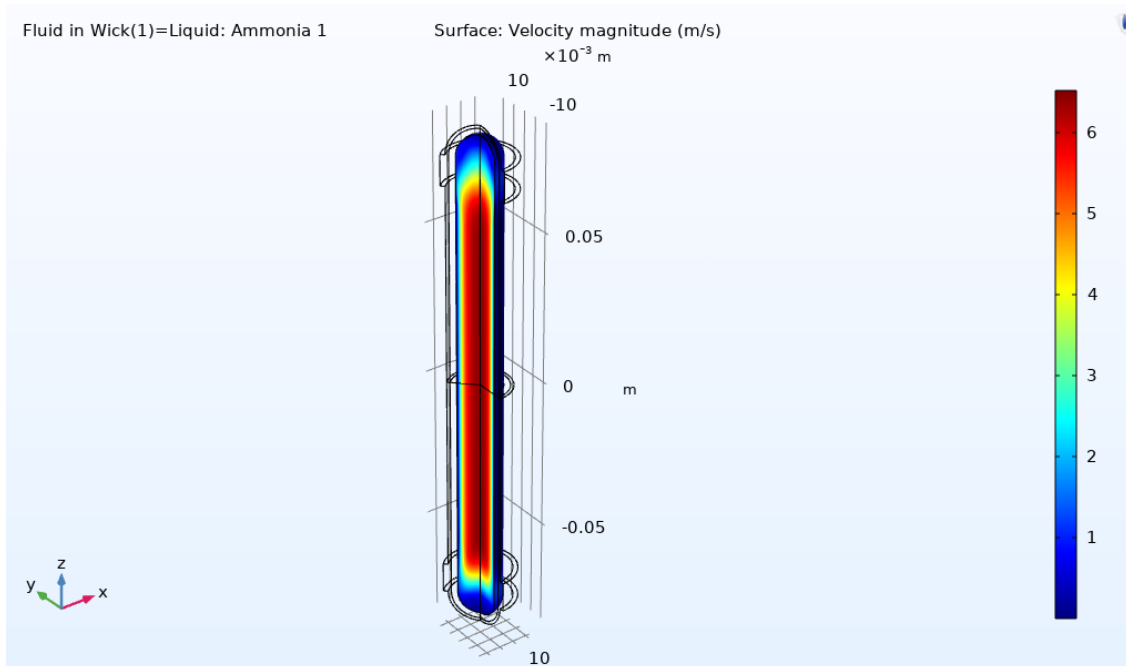


Figure 16. Velocity profile in internal cavity

The estimated velocity fields , as well as the temperature throughout the geometry, are presented beside each other in Figure 17.

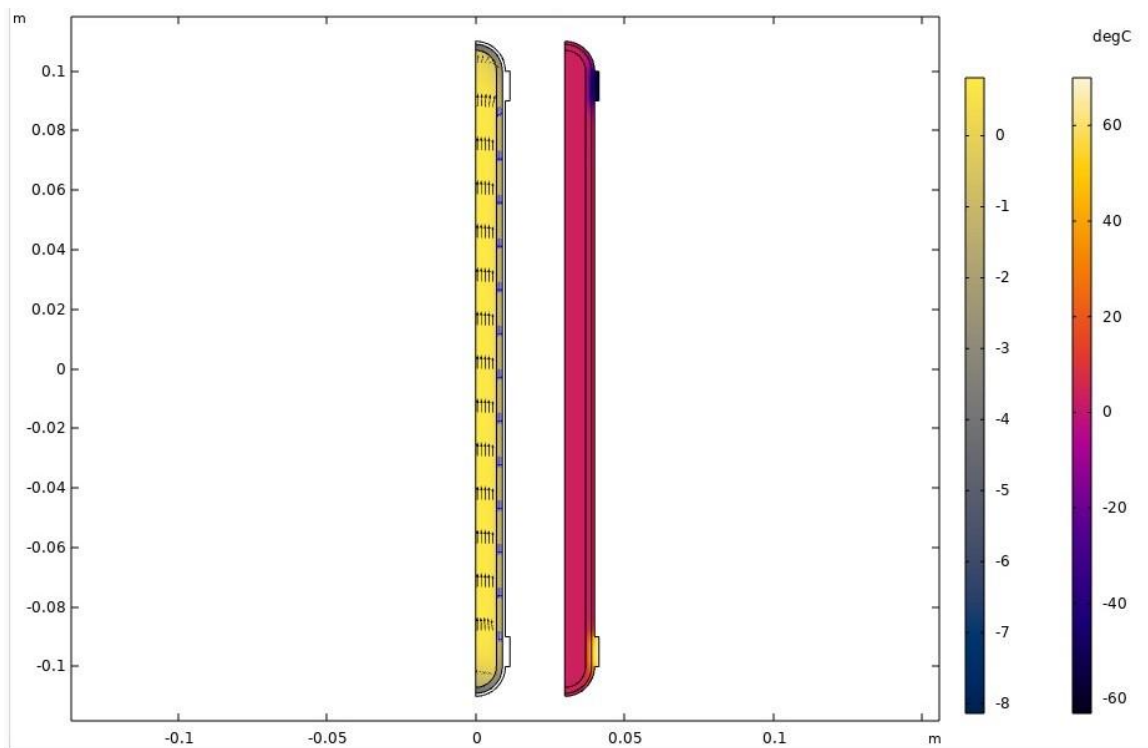


Figure 17. Fluid velocities and temperature in the heat pipe running at the design point. Inside a heat pipe, it can be seen that velocities of higher magnitudes depicted by the larger arrows. The heat pipe successfully conveyed hot vapor to condensed fluid, according to the temperature distribution study in Figure 17. The approval of a pipe with an internal wick structure allows boiling and condensation to occur inside the pipe, which leads to heat transfer from the hot end to the cooled end, which is once again proved in this simulation. As it can be seen, the heat dispersion is smooth.

As it was mentioned before, numerical simulations was used to clarify the significance of key parameters in heat pipe design by providing parametric analysis. From the FE model the heat flow rate was calculated (see Figure 18) and the coefficient is obtained for further lumped parameter model.

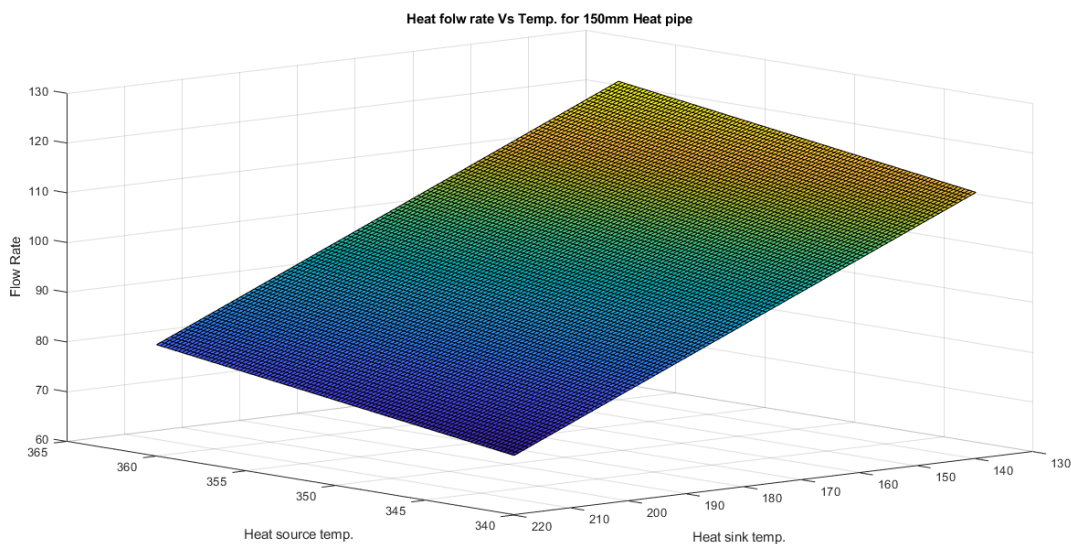


Figure 18. Heat flow rate and Temperature relation.

6.2. Lumped parameter model

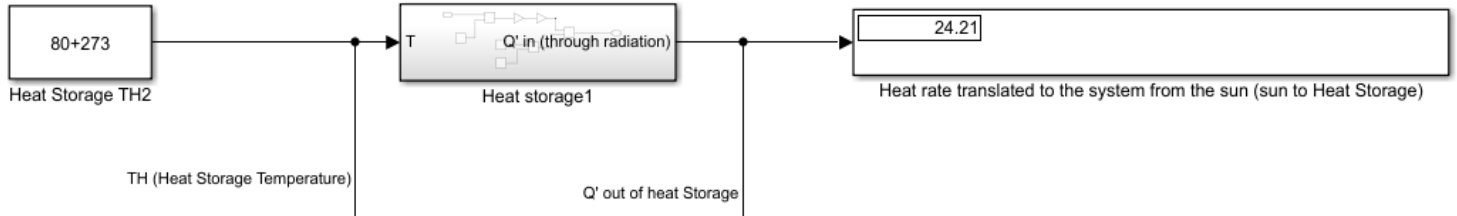


Figure 19. Lumped model-part 1

Figure 19 shows the heat radiated to the heat storage, it shows that this subsystem gets 24.21W from the solar radiation to keep it at 80°C. This heat is totally translated to the battery through the heat pipe. The surface area of the heat storage is $0.202 \times 0.3 \text{ m}^2$.

Based on the radiation analysis, the temperature of the heat storage is known, in addition, the heat flow rate translated to heat storage from the sun is calculated. This amount of heat flow rate is totally translated to the battery. For the battery, the coming heat flow rate and the source temperature is known, therefore, the battery temperature can be calculated.

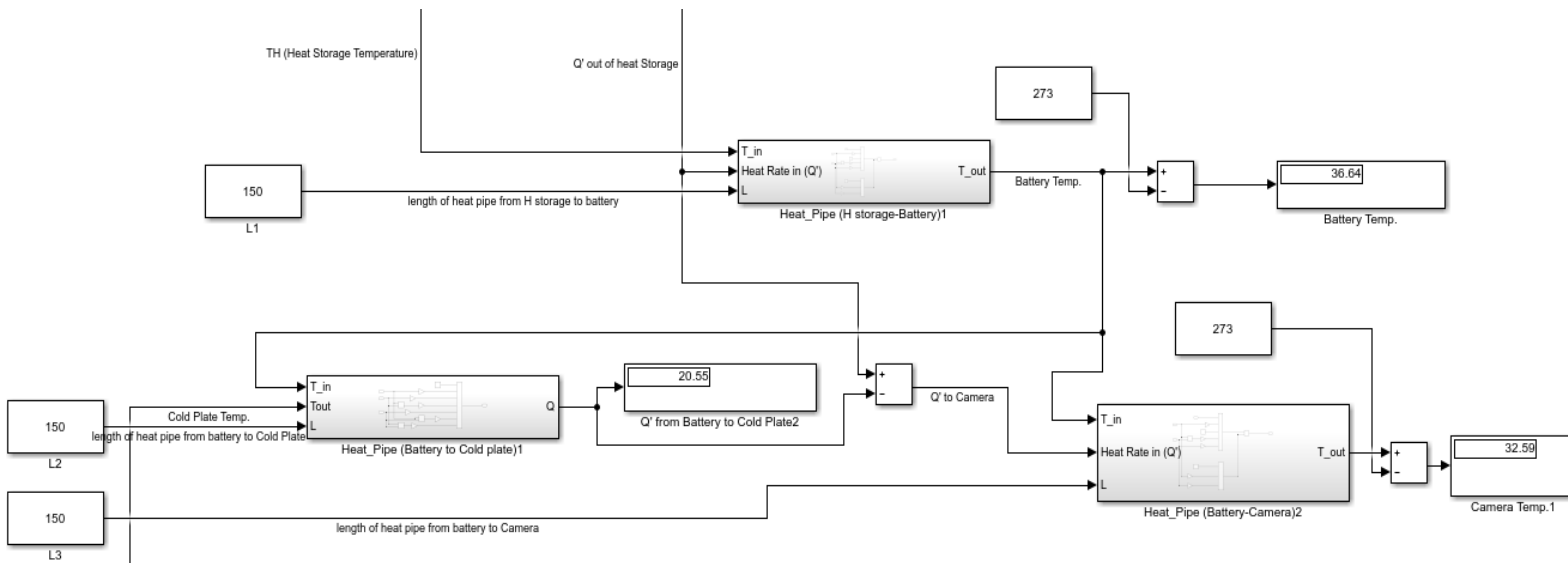


Figure 20. Lumped model-part 2

Knowing the battery temperature and the cold plate temperature is assumed to be at 0 degree Celsius, therefore, the heat flow rate from battery to the cold plate can be calculated using the first representation of the heat pipe. The rest of heat flowrate is translated to the camera so the second representation of heat pipe can be used for calculating the camera temperature.

Figure 20 shows the results of temperature and heat flow rate among heat storage, battery, camera and cold plate network. Firstly, 24.21W is translated from heat storage to the battery, then, 20.55W of this flow rate is translate from the battery to the cold plate and the rest flow rate is translated to camera then to the cold plate. All the heat translation in this network is through heat pipes of 150mm length. The temperature of battery is calculated at 36.64°C and temperature of the camera is at 32.59°C.

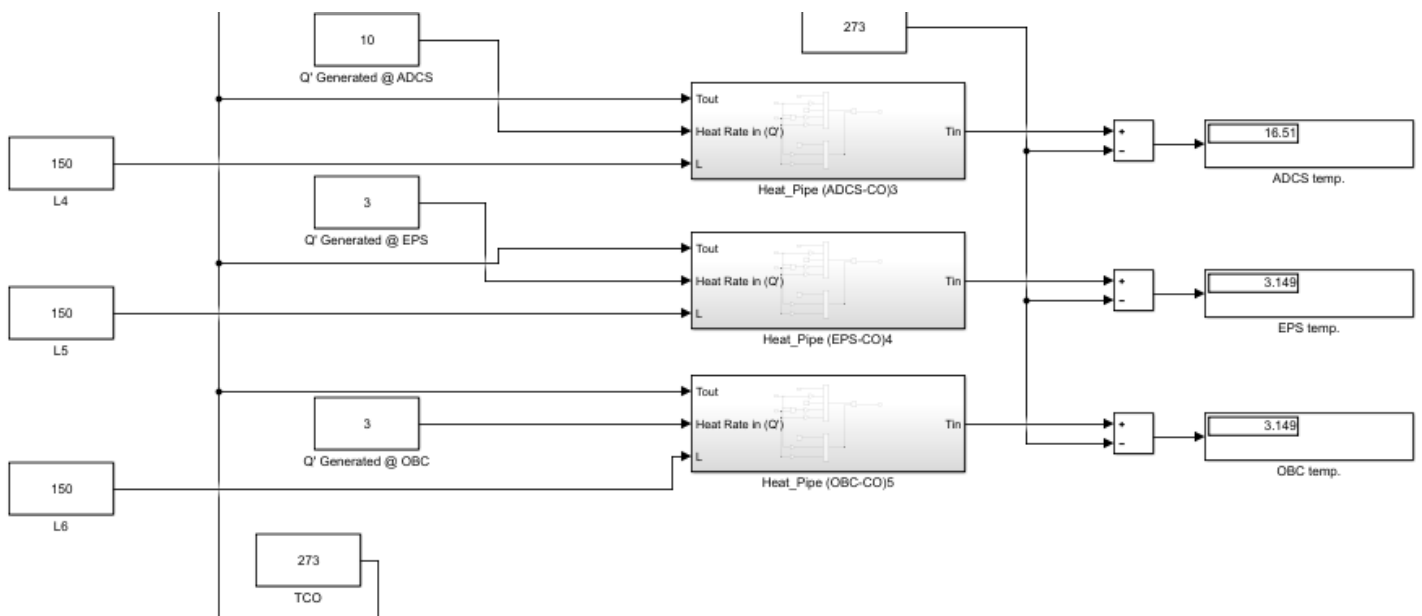


Figure 21. Lumped model-part 3

For the heat generating subsystems, the heat flowrate at each subsystem is assumed based on the literature. Therefore, the heat flow rate is known, in addition, by knowing the cold plate

temperature, the temperature of each subsystem can be calculating using the third representation of the heat pipe(Figure 21).

Figure 21 shows the final section of the heat transfer network which shows the generating heat subsystems, for the ADCS (attitude determination and control), it generates power of 10W, this power is translated totally to the cold plate and keep its temperature at 16.51°C, the EPS (electrical power system) and OBC (on board computers) generate 3W and their temperature is kept at 3.14°C. The used heat pipes have a length of 150mm.

The temperature and heat flow rate calculated for each subsystem is represented below and based on the literature it satisfy the operational range [45]. All the Heat addition through heat storage, ADCS, EPS and OBC is extracted through the cold plate.

Subsystem	Temperature (°C)	Heat Flowrate (W)
Heat Storage	80	24.21
Battery	36.64	24.21
Camera	32.59	3.66
ADCS	16.51	10
EPS	3.149	3
OBC	3.149	3
Cold Plate	0	40.21

Table 3. Subsystem's temperatures and heat flow rate.

The main uncertainty of the model is in the heat pipe section, therefore, if we could assure that the COMSOL model is giving a realistic data, therefore, we can verify that the whole lump model is valid to be used. To check the data of the COMSOL model we need to make some experiments and comparing the outputs of the FE model in COMSOL with the practical data. The other way is checking the trends of the outputs with each inputs parameter and see if it's obeying the physical laws or not.

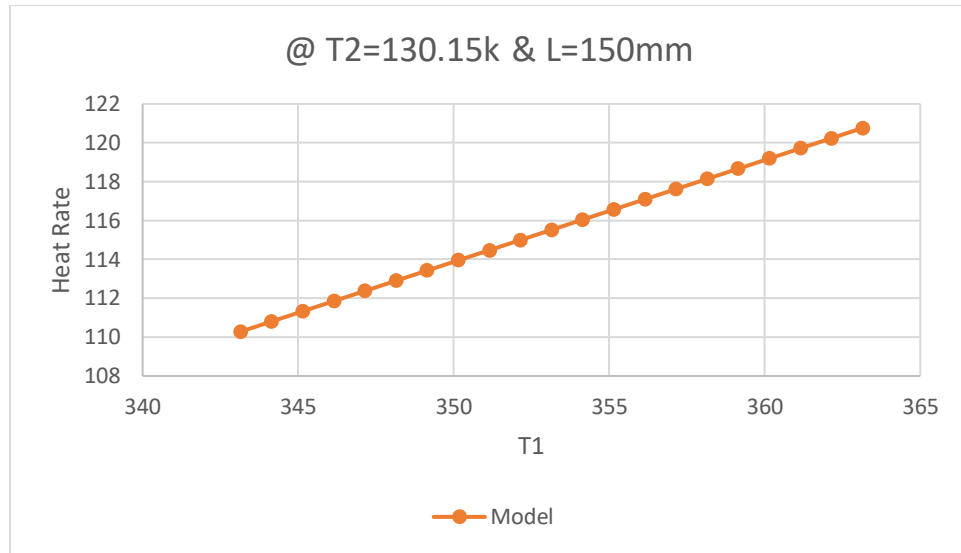


Figure 22. Temperature at the heat sink vs Heat flow rate.

Figure 22 shows the trends of the heat flow rate with the heat source temperature (T_1) while the heat sink temperature (T_2) is fixed at 130.15k for a pipe length of 150mm. The data shows that the heat flow rate is linearly dependent on (T_1). This is physically justified as the heat transfer inside the heat pipe is only conduction and convection which is linearly dependent on the temperature difference ($T_1 - T_2$)

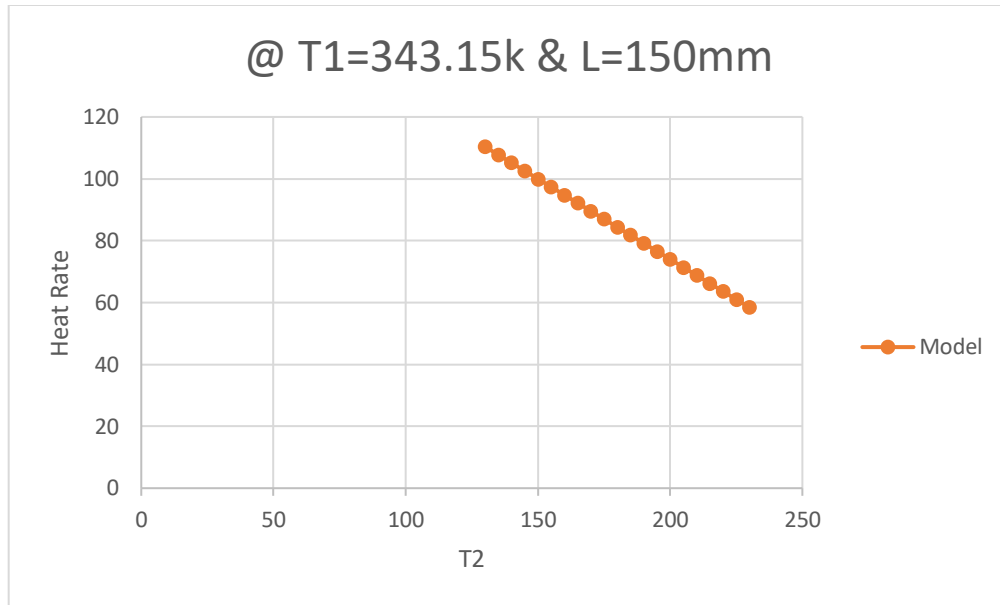


Figure 23. Temperature at the heat source vs Heat flow rate.

Figure 23 shows the trend of Q' with changing T_2 while T_1 is fixed at 343.15k for the same heat pipe (150mm). Based on the model, the heat flow rate is linearly decreasing while increasing the heat sink temperature (T_2). This is also justified physically, the reason for that is, as discussed in the previous chart, the heat flow rate is dependent on temperature difference ($T_1 - T_2$), therefore, while increasing T_2 the difference will decrease so Q' will decrease.

Based on the previous analysis, it can be concluded that the COMSOL model gives a realistic output, therefore, the whole lumped model is practical.

Chapter 7 – Comparison with Mathematical model

After building the FE model using COMSOL, this model is fitted using response surface algorithm to get a mathematical model that will be easy to be used in the lumped parameter model is SIMULINK.

The design of experiments technique (Taguchi Method) is used to plan for the arrangement of the parameters with each other. The design parameters are selected as following

$$T1 \text{ (the heat source temperature)} = 343.15 - 363.15^{\circ}C$$

$$T2 \text{ (the heat Sink Temperature)} = 130.15 - 210.15^{\circ}C$$

$$L \text{ (length of the heat pipe)} = 150 - 1000mm$$

Therefore, there are 3 factors, each factor is changed on two level (as the system is expected to be linear with these parameters) so the chosen orthogonal array, suitable for these factors, is L8OA. The parameters are arranged in L8OA as follow, where (1) stands for the first level, and (2) stands for the second.

Run order	Temperature at the heat sink (T_{sink})	Temperature at the heat source (T_{source})	Interaction of $T_{sink} * T_{source}$	Length of the heat pipe (L)	Interaction of $T_{sink} * L$	Interaction of $T_{source} * L$	Output (Q')
1	130.15	343.15	444660.97	150	19522.5	51472.5	110.290307
2	130.15	343.15	444660.97	1000	130150	343150	110.282151
3	210.15	343.15	72112.97	150	31522.5	51472.5	68.72769536
4	210.15	343.15	72112.97	1000	210150	343150	68.72485452
5	130.15	363.15	47263.97	150	19522.5	54472.5	120.7690334
6	130.15	363.15	47263.97	1000	130150	363150	120.7625718
7	210.15	363.15	76315.97	150	31522.5	54472.5	79.14125766
8	210.15	363.15	76315.97	1000	210150	363150	79.13806139

Table 5. Orthogonal array parameters

After that, the response surface algorithm (attached in the commented MATLAB code in appendix1) is applied to get the algebraic equation that simulating the mathematical model. The output equation is as follow,

$$Q' = A + BT_1 + CT_2 + DT_1T_2 + EL + FLT_1 + GLT_2$$

Where,

$$A = -3.7341$$

$$B = 0.5293$$

$$C = -0.5053$$

$$D = -4.1368E^{-05}$$

$$E = -3.0722E^{-05}$$

$$F = 3.9393E^{-08}$$

$$G = 6.3095E^{-08}$$

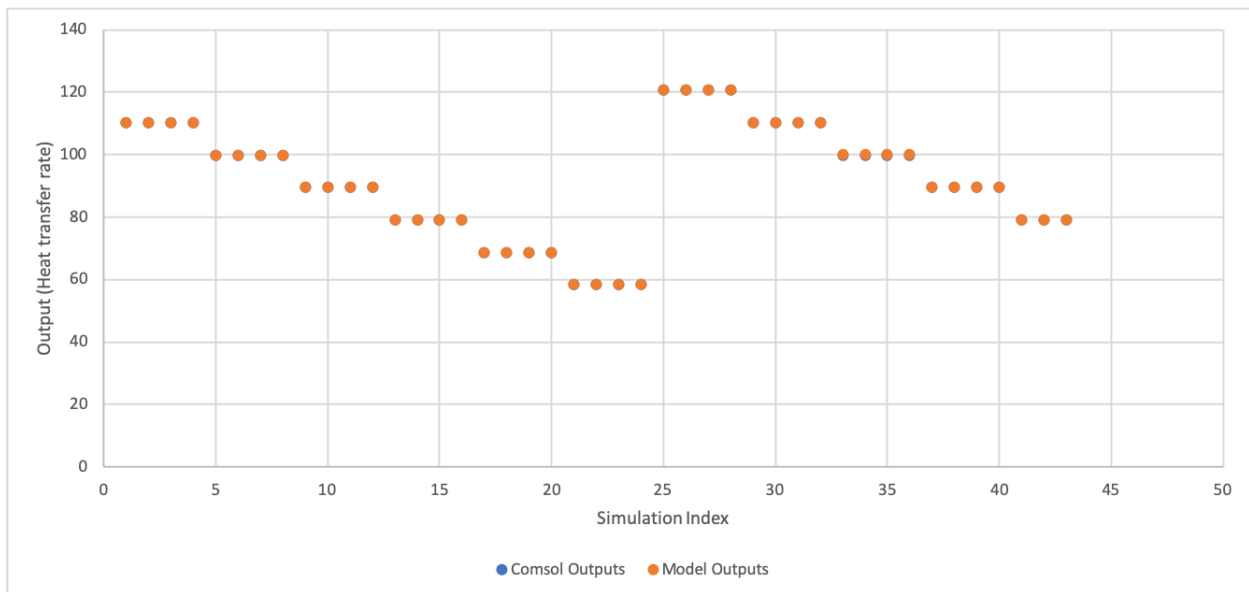


Figure 24. Comsol output vs Mathematical model output

Another set of simulations were accomplished by changing the values of the predefined parameter (simulation outputs is listed in appendix 2). The simulations' output is compared with

the outputs of the mathematical model to verify that the model represents the FE model correctly. The comparison shows average error of 0.016976744% which is very low value(see Figure 24).

Chapter 8 – Conclusions

To conclude, a numerical finite element model presented in order to simulate the thermal model of a heat pipe. Based on that a lumped parameter model was developed further as an engineering-approach tool for the better thermal management of the satellite. A lumped parameter model is found to be the best choice for this purpose rather than conducting a complete CFD and FE analysis for the network which will be time consuming and need high computational power. In the lumped parameter model, each subsystem is modeled using a single block. For the heat pipe, CFD analysis is done for a single heat pipe 8 times and the model is fitted to a mathematical equation to be used in the lumped model. Finally, this equation is verified by comparing it with many other CFD analysis (appendix 2) .

The model of the heat pipe is made for three input parameters (T1, T2 & L). In further developments, there can be futuristic modification to make the model more generic by adding other parameters as pipe outer and internal diameter (D & d), the wick thickness (t) and the wick porous emissivity (e). Therefore, we will have 7 parameters with 2 levels, so there will be a need more simulations($2^7=128$) to get accurate model using Taguchi and response surface technique.

References

- [1] S. J. Dong, Y. Z. Li, J. Wang, and J. Wang, “Fuzzy incremental control algorithm of loop heat pipe cooling system for spacecraft applications,” *Comput. Math. with Appl.*, vol. 64, no. 5, pp. 877–886, 2012, doi: 10.1016/j.camwa.2012.01.030.
- [2] C. Hoa, B. Demolder, and A. Alexandre, “Roadmap for developing heat pipes for ALCATEL SPACE’s satellites,” *Appl. Therm. Eng.*, vol. 23, no. 9 SPEC., pp. 1099–1108, 2003, doi: 10.1016/S1359-4311(03)00039-5.
- [3] G. Cluzet, “(12) Patent Application Publication (10) Pub. No.: US 2004/0040691 A1,” vol. 1, no. 19, 2004.
- [4] P. D. Tegenaw, M. G. Gebrehiwot, and M. Vanierschot, “On the comparison between computational fluid dynamics (CFD) and lumped capacitance modeling for the simulation of transient heat transfer in solar dryers,” *Sol. Energy*, vol. 184, no. March 2018, pp. 417–425, 2019, doi: 10.1016/j.solener.2019.04.024.
- [5] X. Cui *et al.*, “Optimization of the lumped parameter thermal model for hard-cased li-ion batteries,” *J. Energy Storage*, vol. 32, no. March, p. 101758, 2020, doi: 10.1016/j.est.2020.101758.
- [6] P. Nemeč, A. Čaja, and M. Malcho, “Mathematical model for heat transfer limitations of heat pipe,” *Math. Comput. Model.*, vol. 57, no. 1–2, pp. 126–136, 2013, doi: 10.1016/j.mcm.2011.06.047.
- [7] M. Ando *et al.*, “On-orbit demonstration of oscillating heat pipe with check valves for space application,” *Appl. Therm. Eng.*, vol. 130, pp. 552–560, 2018, doi: 10.1016/j.applthermaleng.2017.11.032.
- [8] V. Venkataraman, “Thermal modelling and coupling of a heat pipe integrated desorber with a Solid Oxide Fuel Cell,” *Appl. Therm. Eng.*, vol. 147, no. October 2018, pp. 943–961, 2019, doi: 10.1016/j.applthermaleng.2018.10.131.
- [9] Y. Gan, J. Wang, J. Liang, Z. Huang, and M. Hu, “Development of thermal equivalent circuit model of heat pipe-based thermal management system for a battery module with cylindrical cells,” *Appl. Therm. Eng.*, vol. 164, no. October 2019, p. 114523, 2020, doi: 10.1016/j.applthermaleng.2019.114523.
- [10] K. Desai, G. Lakra, R. Rajesh, and S. Senthur Prabu, “Investigation on the effect of thermal properties by changing geometry of a heat pipe using simulation,” *Mater. Today Proc.*, vol. 46, no. xxxx, pp. 8473–8479, 2021, doi: 10.1016/j.matpr.2021.03.491.
- [11] L. Pietrasanta, G. Postorino, R. Perna, M. Mameli, and S. Filippeschi, “A pulsating heat pipe embedded radiator: Thermal-vacuum characterisation in the pre-cryogenic temperature range for space applications,” *Therm. Sci. Eng. Prog.*, vol. 19, no. June, p.

- 100622, 2020, doi: 10.1016/j.tsep.2020.100622.
- [12] L. L. Vasiliev, “Micro and miniature heat pipes - Electronic component coolers,” *Appl. Therm. Eng.*, vol. 28, no. 4, pp. 266–273, 2008, doi: 10.1016/j.applthermaleng.2006.02.023.
- [13] C. B. VanOutryve, “A thermal analysis and design tool for small spacecraft,” *Aerosp. Sci. Technol.*, p. 125, 2008, [Online]. Available: https://scholarworks.sjsu.edu/etd_theses/3619.
- [14] H. Hale and P. R. S. Shelke, “METHODS OF ENHANCEMENT OF HEAT TRANSFER THROUGH HEAT PIPE- A REVIEW,” pp. 93–100.
- [15] Т. П. Университет, “1 БМ4В Руководитель,” pp. 1–144, 2016.
- [16] J. Duffy and J. W. Wang, “Heat Pipe Application,” no. August, pp. 807–813, 2007.
- [17] K. El-kobba, “TH-o3 529,” no. May, pp. 17–19, 2005.
- [18] P. M. Dussinger and W. G. Anderson, “Design and Testing of Titanium / Cesium and Titanium / Potassium Heat Pipes,” no. September, pp. 1–9, 2015.
- [19] S. S. Sandeep and S. B. Prakash, “Design of heat pipe based on capillary and entrainment limitations,” *AIP Conf. Proc.*, vol. 2200, no. January 2020, 2019, doi: 10.1063/1.5141239.
- [20] B. Richard, D. Pellicone, and W. G. Anderson, “Loop Heat Pipe Wick Fabrication via Additive Manufacturing TFAWS Active Thermal Paper Session Background,” 2017.
- [21] E. F. Moura, I. B. Henriques, and G. B. Ribeiro, “Thermodynamic modeling and exergy analysis of a stirling cycle for space power generation,” *ECOS 2020 - Proc. 33rd Int. Conf. Effic. Cost, Optim. Simul. Environ. Impact Energy Syst.*, no. June, pp. 424–436, 2020.
- [22] C. Y. Tseng, K. S. Yang, and C. C. Wang, “Non-uniform three-dimensional pulsating heat pipe for anti-gravity high-flux applications,” *Energies*, vol. 13, no. 12, pp. 1–16, 2020, doi: 10.3390/en13123068.
- [23] M. Tunzi, M. Ruyschaert, S. Svendsen, and K. M. Smith, “Double loop network for combined heating and cooling in low heat density areas,” *Energies*, vol. 13, no. 22, 2020, doi: 10.3390/en13226091.
- [24] L. E. M. Alexandre, “THERMAL MODELING OF SATELLITES,” 2016.
- [25] J. Lee, D. Kim, J. Mun, and S. Kim, “Heat-transfer characteristics of a cryogenic loop heat pipe for space applications,” *Energies*, vol. 13, no. 7, 2020, doi: 10.3390/en13071616.
- [26] Y. Ma *et al.*, “Neutronic and thermal-mechanical coupling analyses in a solid-state reactor using Monte Carlo and finite element methods,” *Ann. Nucl. Energy*, vol. 151, no. November, p. 107923, 2021, doi: 10.1016/j.anucene.2020.107923.
- [27] N. Blet, S. Lips, and V. Sartre, “Heats pipes for temperature homogenization : A literature

review To cite this version : HAL Id : hal-01487695,” 2019.

- [28] M. Gulde, J. M. Mancías, C. De Genova, M. Schimmerohn, and F. Schäfer, “Reliable , Fast , and Flexible : A Thermal Modeling Approach for Small Satellites,” *32nd Annu. AIAA/USU Conf. Small Satell.*, 2018.
- [29] M. Gadalla, M. Ghommem, G. Bourantas, and K. Miller, “Modeling and thermal analysis of a moving spacecraft subject to solar radiation effect,” *Processes*, vol. 7, no. 11, pp. 1–15, 2019, doi: 10.3390/pr7110807.
- [30] T. Management, “Integrated Heat Pipe Technology for Thermal Management of Electronics,” *Qpedia*, no. March 2012, 2013.
- [31] P. Golda, R. Schießl, and U. Maas, “Heat transfer simulation of a cryogenic cooling stream in machining operation,” *Int. J. Heat Mass Transf.*, vol. 144, p. 118616, 2019, doi: 10.1016/j.ijheatmasstransfer.2019.118616.
- [32] D. W. Hengeveld, M. M. Mathison, J. E. Braun, E. A. Groll, and A. D. Williams, “Review of modern spacecraft thermal control technologies,” *HVAC R Res.*, vol. 16, no. 2, pp. 189–220, 2010, doi: 10.1080/10789669.2010.10390900.
- [33] J. V. Suresh and P. Bhramara, “CFD Analysis of Copper Closed Loop Pulsating Heat pipe,” *Mater. Today Proc.*, vol. 5, no. 2, pp. 5487–5495, 2018, doi: 10.1016/j.matpr.2017.12.138.
- [34] C. An and J. Su, “Lumped models for transient thermal analysis of multilayered composite pipeline with active heating,” *Appl. Therm. Eng.*, vol. 87, pp. 749–759, 2015, doi: 10.1016/j.applthermaleng.2015.05.061.
- [35] D. Beard, W. G. Anderson, and C. Tarau, “Self-venting arterial heat pipes for spacecraft applications,” *14th Int. Energy Convers. Eng. Conf. 2016*, pp. 1–14, 2016.
- [36] K. P. Ivanov and E. G. Bournaski, “Combined distributed and lumped parameters model for transient flow analysis in complex pipe networks,” *Comput. Methods Appl. Mech. Eng.*, vol. 130, no. 1–2, pp. 47–56, 1996, doi: 10.1016/0045-7825(95)00894-2.
- [37] P. Alto, “Trochi,” vol. 1, no. 12, 2004.
- [38] K. H. W. Seah, X. Li, and K. S. Lee, “The effect of applying coolant on tool wear in metal machining,” *J. Mater. Process. Tech.*, vol. 48, no. 1–4, pp. 495–501, 1995, doi: 10.1016/0924-0136(94)01688-W.
- [39] D. A. Reay, “Thermal energy storage: The role of the heat pipe in performance enhancement,” *Int. J. Low-Carbon Technol.*, vol. 10, no. 2, pp. 99–109, 2015, doi: 10.1093/ijlct/ctv009.
- [40] D. Dinh, “Thermal modeling of a nanosat,” no. May, 2012.
- [41] W. Street, “(12) United States Patent,” vol. 1, no. 7, 2001.

- [42] M. Bonnici, P. Mollicone, M. Fenech, and M. A. Azzopardi, “Analytical and numerical models for thermal related design of a new pico-satellite,” *Appl. Therm. Eng.*, vol. 159, no. October 2018, p. 113908, 2019, doi: 10.1016/j.applthermaleng.2019.113908.
- [43] E. Hazir and K. H. Koc, “Optimization of wood machining parameters in CNC routers: Taguchi orthogonal array based simulated angling algorithm,” *Maderas Cienc. y Tecnol.*, vol. 21, no. 4, pp. 493–510, 2019, doi: 10.4067/s0718-221x2019005000406.
- [44] S. Selvadurai, A. Chandran, D. Valentini, and B. Lamprecht, “applied sciences Passive Thermal Control Design Methods , Analysis , Comparison , and Evaluation for Micro and Nanosatellites Carrying Infrared Imager,” 2022.
- [45] M. Theses and K. E. Boushon, “Scholars ’ Mine Thermal analysis and control of small satellites in low Earth orbit Presented to the Faculty of the Graduate School of the In Partial Fulfillment of the Requirements for the Degree,” 2018.
- [46] T. Brahim and A. Jemni, “Heat Pipe Simulation Under Critical Conditions,” *Front. Heat Pipes*, vol. 3, no. 3, 2013, doi: 10.5098/fhp.v3.3.3003.

Appendices

Appendix 1:

```
T11=343.15; %1st level of T1
T21=130.15; %1st level of T2
T12=363.15; %2nd level of T1
T22=210.15; %2nd level of T2
L1=150;      %1st level of L
L2=1000;     %2nd level of L

z1=ones(8,1);

%Z is the arrangement of parameters in L8 Orthogonal array
z=[T11 T21 T11*T21 L1 T11*L1 T21*L1;
   T11 T21 T11*T21 L2 T11*L2 T21*L2;
   T11 T22 T11*T22 L1 T11*L1 T22*L1;
   T11 T22 T11*T22 L2 T11*L2 T22*L2;
   T12 T21 T12*T21 L1 T12*L1 T21*L1;
   T12 T21 T12*T21 L2 T12*L2 T21*L2;
   T12 T22 T12*T22 L1 T12*L1 T22*L1;
   T12 T22 T12*T22 L2 T12*L2 T22*L2];

z=[z1 z];

% is the output column in the orthogonal array
F=[110.290307;
   110.2821506;
```

```

68.72769536;
68.72485452;
120.7690334;
120.7625718;
79.14125766;
79.13806139];

% B is the coefficients of the output equation
% Q_dot = B(1) + B(2)*T1 + B(3)*T2 + B(4)*T1*T2
%           + B(5)*L + B(6)*L*T1 + B(7)*L*T2
B=inv(z'*z)*z'*F;

```

Appendix 2:

T1 (K)	T2 (K)	L (mm)	Q' (W) (Simulation)	Q' (w) (Math. Model)	Error %
343.15	130.15	150	110.2903	110.281516	0.01
343.15	130.15	500	110.2889	110.2783687	0.01
343.15	130.15	1000	110.2822	110.2738724	0.01
343.15	130.15	1500	110.279	110.2693762	0.01
343.15	150.15	150	99.87642	99.89179672	0.02
343.15	150.15	500	99.87595	99.88909102	0.01
343.15	150.15	1000	99.87094	99.88522573	0.01
343.15	150.15	1500	99.86935	99.88136044	0.01
343.15	170.15	150	89.48121	89.50207742	0.02
343.15	170.15	500	89.4811	89.49981338	0.02
343.15	170.15	1000	89.477	89.49657904	0.02

343.15	170.15	1500	89.4763	89.4933447	0.02
343.15	190.15	150	79.0989	79.11235812	0.02
343.15	190.15	500	79.09892	79.11053575	0.01
343.15	190.15	1000	79.09547	79.10793236	0.02
343.15	190.15	1500	79.09483	79.10532897	0.01
343.15	210.15	150	68.7277	68.72263882	0.01
343.15	210.15	500	68.72778	68.72125811	0.01
343.15	210.15	1000	68.72485	68.71928568	0.01
343.15	210.15	1500	68.72456	68.71731324	0.01
343.15	230.15	150	58.36682	58.33291952	0.06
343.15	230.15	500	58.36695	58.33198048	0.06
343.15	230.15	1000	58.36449	58.33063899	0.06
343.15	230.15	1500	58.36429	58.3292975	0.06
363.15	130.15	150	120.769	120.7599533	0.01
363.15	130.15	500	120.7685	120.7570817	0.01
363.15	130.15	1000	120.7626	120.7529794	0.01
363.15	130.15	1500	120.7606	120.7488771	0.01
363.15	150.15	150	110.342	110.3536868	0.01
363.15	150.15	500	110.3418	110.3512568	0.01
363.15	150.15	1000	110.3369	110.3477855	0.01
363.15	150.15	1500	110.3356	110.3443141	0.01
363.15	170.15	150	99.93022	99.94742029	0.02
363.15	170.15	500	99.93016	99.94543201	0.02
363.15	170.15	1000	99.92593	99.9425916	0.02
363.15	170.15	1500	99.92509	99.93975119	0.01
363.15	190.15	150	89.53036	89.5411538	0.01

363.15	190.15	500	89.53035	89.53960717	0.01
363.15	190.15	1000	89.52665	89.53739772	0.01
363.15	190.15	1500	89.52604	89.53518826	0.01
363.15	210.15	150	79.14126	79.1348873	0.01
363.15	210.15	500	79.14128	79.13378234	0.01
363.15	210.15	1000	79.13806	79.13220383	0.01